Comparative study of force computation methods for acoustic analyses of electrical machines

Michael van der Giet*, David Franck*, François Henrotte*, and Kay Hameyer*

*Institute of Electrical Machines, RWTH Aachen University, Schinkelstraße 4, D-52056 Aachen, Germany
E-mail: MvdG@iem.rwth-aachen.de

***Abstract*—A comparison of different force calculation methods with practical application to vibro-acoustical problems of electrical machines is performed. A formula is derived to directly determine force waves from nodal forces and a test case is proposed to study the convergence behavior of the discretization error. An analytical model is used to determine radial vibration. Torque ripple is also considered. It is found that nodal forces show an equal convergence rate, when compared to other methods, but give better performance in terms of discretization noise.**

***Index Terms*—Numerically weak magneto-mechanical coupling, acoustics of electrical machines, noise and vibration**

I. Introduction

The acoustic behavior of electrical machines is of interest. Using 2D Finite Element analyses, the magnetic field is determined, from which the magnetic force excitations in mode/frequency domain are to be determined. Four different methods to do so are studied in this paper.

Electromagnetic forces are causing an exchange of energy between the electromagnetic and the mechanical compartment. Therefore, the energy based formulation, presented in [1], is used to derive expressions for the calculation of electromagnetic forces.

The change of magnetic energy that is converted into mechanical energy can be written as the tensor product ($\mathbf{a} : \mathbf{b} = \sum_{i,j} a_{ij} b_{ij}$) of a stress tensor $\boldsymbol{\sigma}_{\mathrm{EM}}$ and the gradient of the velocity field $\nabla\mathbf{v}$:

$$\dot{W}_{\mathrm{M}} = \int_{\Omega} \boldsymbol{\sigma}_{\mathrm{M}} : \nabla\mathbf{v}\, \mathrm{d}\Omega. \tag{1}$$

The electromechanical stress tensor is identified as:

$$\boldsymbol{\sigma}_{\mathrm{M}} = \mathbf{b}\tilde{\mathbf{h}} - \{\tilde{\mathbf{h}} \cdot \mathbf{b} - \rho_{\mathrm{M}}^{W}(\mathbf{b})\}\mathbb{I}. \tag{2}$$

Integrating (1) by part gives

$$\int_{\Omega} \boldsymbol{\sigma}_{\mathrm{M}} : \nabla\mathbf{v}\mathrm{d}\Omega = -\int_{\Omega} \rho_{\mathrm{M}}^{\mathbf{f}} \cdot \mathbf{v}\mathrm{d}\Omega + \int_{\partial\Omega} \mathbf{n} \cdot \boldsymbol{\sigma}_{\mathrm{M}} \cdot \mathbf{v}\mathrm{d}\partial\Omega, \tag{3}$$

where the electromagnetic volume force density $\rho_{\mathrm{M}}^{\mathbf{f}} = \nabla \cdot \sigma_{\mathrm{M}}$ is the divergence of the stress tensor. For $\boldsymbol{\sigma}_{\mathrm{M}}$ is discontinuous at material interfaces, distributions theory [2] can be used to define a surface-force density $\Delta\boldsymbol{\sigma}_{\mathrm{M}}$ at the interface as divergence in the sense of distribution (also sometimes referred to as surface divergence [3]):

$$\Delta\boldsymbol{\sigma}_{\mathrm{M}} = \mathrm{Div}\boldsymbol{\sigma}_{\mathrm{M}} = \lim_{A\to 0} \frac{1}{A} \oint_{A} \boldsymbol{\sigma}_{\mathrm{M}} \cdot \mathbf{n}\mathrm{d}A\,, \tag{4}$$

where A is the area of a volume at the surface, which is partly located in material 1 and partly in material 2. Evaluating the limit, it can be shown that the surface force density is normal to the material interface between the material 1 and 2 and that it is given by [4]

$$\Delta\boldsymbol{\sigma}_{\mathrm{M}} = (\boldsymbol{\sigma}_{\mathrm{M2}} - \boldsymbol{\sigma}_{\mathrm{M1}}) \cdot \mathbf{n}_{12}\,, \tag{5}$$

where $\mathbf{n}_{12}$ is the normal vector from material 1 to material 2 and $\boldsymbol{\sigma}_{\mathrm{M1}}$ and $\boldsymbol{\sigma}_{\mathrm{M2}}$ are the stress tensors of material 1 and 2, respectively.

Regarding the electro-mechanical coupling, the following assumption is made in this paper: The reaction of mechanical deformation on the electromagnetic field is negligible. This implies that the structure can be considered as a rigid body for the electromagnetic force calculation. In this case, the gradient of the velocity field $\nabla\mathbf{v}$ is zero everywhere in the material. Therefore, the resultant force $\int_{\Omega} \rho_{\mathrm{M}}^{\mathbf{f}} \cdot \mathrm{d}\Omega$ is equal to the surface integral of the stress tensor $\int_{\partial\Omega} \mathbf{n} \cdot \sigma_{\mathrm{M}} \cdot \mathrm{d}\partial\Omega$ in (3).

The numerical simulation of electrical machines with the objective of analyzing vibration and acoustic noise involves the computation of electromagnetic forces as global quantities, acting on the center of gravity, as well as local distributions in space. In electrical machines, the former are mainly electromagnetic torque and global force acting on the shaft, which is also called unbalanced magnetic pull (UMP). The latter one are reluctance surface-force distributions at the interface between the stator iron and the air gap. They are mainly responsible for the excitation of radial vibration of the stator. There exist several calculation methods to determine global, as well as local forces in electrical machines [5], [6], [7].

A general method to electromagnetic force computation, based on the energy view point, is the so called eggshell method [7]: To compute the forces on a rigid body Y in the domain Ω, a virtual velocity field $\mathbf{v} = \gamma\mathbf{v}_0 + \mathbf{w_0} \times \mathbf{r}$ is defined, where $\mathbf{v}_0$ and $\mathbf{w}_0$ are constant and γ is a smooth function, with a value of 1 on Y and 0 on $\partial\Omega$. In the velocity field $\mathbf{v}$, the vectors $\mathbf{v}_0$ and $\mathbf{w}_0$ are arbitrary and linearly independent. Choosing them to be the nodal shape functions of one layer of elements (eggshell) around Y leads to the eggshell method [7]. It can be shown by choosing the virtual velocity field appropriately, that the eggshell method is a generalization of the approach proposed by Arkkio [5] to calculate the electromagnetic torque of cylindrical electrical machines in

2D, which gives

$$\mathbf{T}_Y = \frac{\mathbf{e}_z l_z}{\delta} \int_{D/2-\delta}^{D/2} \int_0^{2\pi} (\boldsymbol{\sigma}_{\mathrm{M}})_{r\alpha} r \, \mathrm{d}r \mathrm{d}\alpha \,, \tag{6}$$

and in its simpler form, which is commonly referred to the MAXWELL'S stress tensor method, given by

$$\mathbf{T}_Y = \mathbf{e}_z l_z \int_0^{2\pi} r (\boldsymbol{\sigma}_{\mathrm{M}})_{r\alpha} r \, \mathrm{d}\alpha \,, \tag{7}$$

where $(\boldsymbol{\sigma}_{\mathrm{M}})_{r\alpha}$ denotes the radial and azimuthal components of the stress tensor and D the diameter of the stator bore.

Another method proposed for electromagnetic force calculation, which is based on the partial derivative of the JACOBIAN of the field problem is known as COULOMB'S method or virtual work method [6]. This method can be obtained taken $\mathbf{v}_0$ as the virtual velocity field of one node k and choosing γ to be the nodal shape function N_k. Then the nodal force is given by the definition as

$$\mathbf{f}_k = \int_\Omega \rho_{\mathrm{M}}^{\mathbf{f}} \gamma \mathrm{d}\Omega = \int_\Omega \nabla \gamma \boldsymbol{\sigma}_{\mathrm{M}} \cdot \mathrm{d}\Omega \,. \tag{8}$$

Total global forces and torque can then be obtained by summation over all nodes of the moving part.

It is essential to determine local force quantities to solve a subsequent structural problem. One method, commonly used to determine radial force distributions in electrical machines is derived from (5)

$$\Delta\boldsymbol{\sigma}_{\mathrm{M}} = \left(\mathbf{b}_{\mathrm{n}} (\mathbf{h}_{\mathrm{n}2} - \mathbf{h}_{\mathrm{n}1}) - (\rho_{\mathrm{M}2}^{W'} - \rho_{\mathrm{M}1}^{W'}) \right) \mathbf{n}_{12}, \tag{9}$$

where material 2 here means stator iron and material 1 has approximately the permeability of vacuum, i.e. copper or air. The magnetic co-energy is denoted by $\rho_{\mathrm{M}}^{W'}$. For linear magnetic material and if the magnetic-field strength in region 2 (iron) is neglected this reduces to the magnetic pressure

$$\Delta\tilde{\boldsymbol{\sigma}}_{\mathrm{M}} = \frac{1}{2} \left(\mathbf{b}_{\mathrm{n}} \mathbf{h}_{\mathrm{n}} \right) \mathbf{n}_{12}. \tag{10}$$

This is sometimes referred to as the simplified MAXWELL stress tensor. Since the surface-force density (9) is normal with respect to the interface, applied to a rotating machine, all force components in the air gap are radial, only force components on the tooth flanks are azimuthal and thus contributing to torque. Therefore, (9) may also be summed up over the stator surface to compute torque

$$\mathbf{T} = \int_{\partial\Omega} \mathbf{r} \times \Delta\boldsymbol{\sigma}_{\mathrm{M}} \cdot \mathrm{d}\partial\Omega \,. \tag{11}$$

However, this is not a common way to compute global force and torque.

The nodal forces, obtained from COULOMB'S method or from the general eggshell method, can directly used as local forces for the structural problem. In addition, the electromechanical stress tensor can itself be used as applied mechanical stress. This states a good starting point for strong magneto-mechanical coupling, as it can be easily implemented in a common equation system.

A. Radial force density waves from numerical simulation

To bring the analytical understanding of electromagnetic force excitations in terms of force waves in conjunction with the accuracy expected from numerical simulations [8], it is desirable to find expressions of the surface-force density in terms of a FOURIER series expansion. Therefore, the force excitation is projected on to the stator bore. In addition, a spatial FOURIER decomposition of the radial force allows for the use of unit-force excitations on a structural mesh [9].

Assuming a 2D model, this gives rise to a 1D interval $\alpha \in [0, 2\pi)$ on which the surface-force density needs to be defined. For 3D model, this becomes a cylinder, which may be sliced into multiple rings along the axial direction. Naturally, the surface force is equal to zero in the slot, which emphasizes the spatial periodicity of the number of stator slots. If the surface force is available as a density, e.g. from (9) or (10), then the FOURIER expansion can be easily found by sampling it along the stator surface and performing a DFT. If the force excitation is given in terms of nodal forces $\mathbf{f}_k$, the force density can be defined using the DIRAC-δ function

$$\sigma_{\mathrm{rad}}(\alpha) = \frac{1}{R l_z} \sum_{k=1}^{K} \mathbf{e}_{\mathbf{r}k} \cdot \mathbf{f}_k \delta(\alpha - \alpha_k) \,, \tag{12}$$

where α_k is the angular position of node k and $\mathbf{e}_{\mathbf{r}k}$ the radial unit-vector at node k. Applying the FOURIER transform and taking into account the integral $\int_{-\infty}^{\infty} f(x)\delta(x - x_0)\mathrm{d}x = f(x_0)$, gives

$$\sigma_r = \frac{1}{2\pi R l_z} \sum_{k=1}^{K} \mathbf{e}_{\mathbf{r}k} \cdot \mathbf{f}_k e^{-\mathrm{j}\alpha_k r} \,. \tag{13}$$

II. APPLICATION EXAMPLE

A simulation study case is proposed. It is based on the electromagnetically effective parts of a PM synchronous machine: A stator considered as laminated sheet stack (M250-AP) with slots, a rotor of the same material, with surface mounted permanent magnets ($\mu_{\mathrm{r}} \approx 1$, $B_{\mathrm{rem}} = 1.17\,\mathrm{T}$). The study case geometry definition is shown in Figure 1 and Table I. The number of stator slots is chosen to be $N_1 = 6$ and the number of magnets is $2p = 4$. The analysis of this geometry as fictive machine has several advantages: First, it is defined by only seven geometrical and two topological parameters. Together with the simple geometry, this reduces the influence of the FE modeling and allows for easy numerical reproduction by other researchers. Second, the fact that radial oriented tooth facets are used, offers an exact separation between radial and azimuthal force components. Though the air gap field contains a lot of harmonics, which is favorable in this case, because force harmonics are of interest here, this design is practically relevant, since a symmetrical three phase winding can be placed into the slots, leading to a tooth-coil winding as described in [10].

III. COMPARISON OF FORCE CALCULATION METHODS AND SENSITIVITY TO SAMPLING LOCATION

The 2D electromagnetic simulation gives the field distribution (Figure 2), which is the basis for all tested force

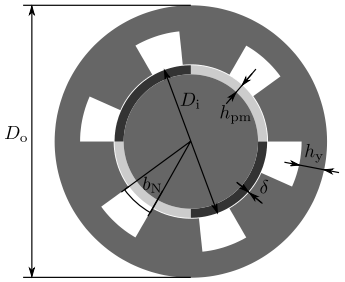

Fig. 1: Geometry of the proposed study case.

TABLE I: Parameters of the proposed study case.

Parameter	Symbol	Value
Number of stator slots	N_1	6
Number of magnets	$2p$	4
Stator outer Diameter	D_o	300 mm
Stator inner Diameter	D_i	170 mm
Air gap	δ	1 mm
Height of yoke	h_y	28 mm
Height of magnets	h_pm	10 mm
Width of the slot opening	b_N	$\frac{2\pi}{15}$ rad
Active length	l_z	400 mm

calculation approaches. The simulation is performed without taking any eddy currents into account. The rotation of the rotor is regarded by means of a moving band width $(\delta/3)$ remeshed at each time step. A total of 400 steps per revolution are to be computed. Due to symmetry and due to the quadratic nature of the electromagnetic forces it suffices to compute only the duration of one pole passing by, i.e. a quarter of a revolution, or 100 steps in this case. Therewith, it is possible to determine forces up to the 200^th higher time harmonic of the fundamental mechanical rotation speed.

To compare the performance of the force calculation approaches, global forces are evaluated as electromagnetic torque and local forces are used to compute the radial force excitation of the stator.

Torque is observed at no-load, which is the cogging torque of the machine, measured as peak-to-peak quantity and as load torque, measured as mean value over one period.

Three different force calculation approaches for the radial force and four approaches for the electromagnetic torque as listed in Table II and III are compared: Nodal forces, surface-force density, MAXWELL'S stress tensor (magnetic pressure) and ARKKIO'S approach [5], where the latter only applies to torque calculation.

To investigate the convergence behavior and to assess the quality of the individual force calculation approaches, force and torque are calculated on meshes with different mesh sizes. The number of degrees-of-freedom (DOF) is increased almost uniformly, and the air gap is always meshed with a higher element density than the rest of the model. Figure 2 shows the surface-force density and the nodal forces on two different meshes. From Figure 2c it can be seen that the surface-force density varies significantly along the tooth edge. There

TABLE II: Global force calculation approaches.

Approach	Global torque
Nodal forces	$\sum_{k=1}^{K} \mathbf{r}_k \times \mathbf{f}_k$
Surface-force density	$\int_{\partial\Omega} \mathbf{r} \times \Delta\boldsymbol{\sigma}_\mathrm{M} \cdot \mathrm{d}\partial\Omega$
MAXWELL'S stress tensor	$\mathbf{e}_z l_z \int_0^{2\pi} (\boldsymbol{\sigma}_\mathrm{M})_{r\alpha} r \mathrm{d}\alpha$
ARKKIO'S approach [5]	$\frac{\mathbf{e}_z l_z}{\delta} \int_{D/2-\delta}^{D/2} \int_0^{2\pi} (\boldsymbol{\sigma}_\mathrm{M})_{r\alpha} r \mathrm{d}r\mathrm{d}\alpha$

TABLE III: Local force calculation approaches.

Approach	Local force
Nodal forces	$\int_\Omega \nabla\gamma\boldsymbol{\sigma}_\mathrm{M} \cdot \mathrm{d}\Omega$
Surface-force density	$(\boldsymbol{\sigma}_\mathrm{M2} - \boldsymbol{\sigma}_\mathrm{M1}) \cdot \mathbf{n}_{12}$
Magnetic pressure	$\approx \frac{1}{2} (\mathbf{b}_\mathrm{n}\mathbf{h}_\mathrm{n}) \mathbf{n}_{12}$

are force peaks at the edges and there is a variation of the cones from one edge to the other. Note that the surface-forces are densities, whereas the nodal forces are net forces (in NEWTON), i.e. the amplitude of the nodal force decreases as the mesh is refined and the amount of nodes increases.

In all cases, it is obvious that the strongest force components occur locally around the singularities at the tooth edge and that the surface-force densities are either radial or azimuthal according to whether they are applied to a facet whose normal is radial or azimuthal, the nodal forces can have azimuthal and radial components at the corner nodes.

Figure 3 shows the convergence behavior of the different global force calculation approaches, in terms of the cogging torque, torque without current on the one hand, and the load torque as mean value in steady-state operation on the other hand. It can be taken that the nodal forces, ARKKIO's approach and the magnetic pressure give approximately the same convergence rate. The only approach, which is converging much slower is the summation of the surface-force density contributions. This can be understood from the fact that only azimuthal components contribute to the electromagnetic torque and the surface-force density is inherently normal to the surface. Therefore, torque contributions only occur at the tooth flanks, where the FE mesh provides a much coarser discretization compared to the air gap.

Since the surface-force density is a local quantity, a norm has to be used to assess the result of the computation as a single value parameter. A natural choice is the stator vibration. At this stage, only the numerical error due to the force calculation is analyzed. Therefore, the force-density waves are weighted by analytical expressions, which are chosen to be the mechanical amplification factors derived by JORDAN [11]. In addition, the frequencies of excitations are proportional to the rotational speed of the machine, which is chosen low enough here to allow disregarding stator resonances and consider only static amplification factors, because the analysis is intended to focus on the force excitation only and the mechanical transfer function is only used inasmuch it is needed to assess the forces. Due to symmetry, no resultant force acting on the rotor occurs in the model. Therefore, the deformation can be described by

$$\underline{u}_r(\omega) = -\frac{RN}{Eh} \underline{\sigma}_r(\omega) \cdot \begin{cases} 1 & \text{for } r = 0 \\ \frac{i^2}{(r^2-1)^2} & r \geq 2 \end{cases}, \qquad (14)$$

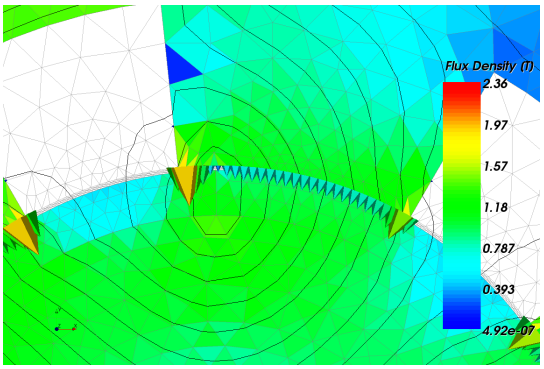

(a) Surface-force density on a coarse mesh.

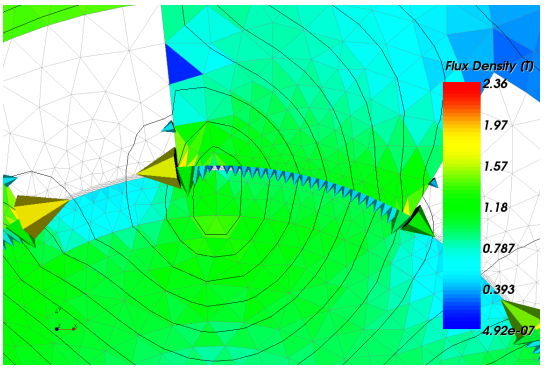

(b) Nodal forces on a coarse mesh.

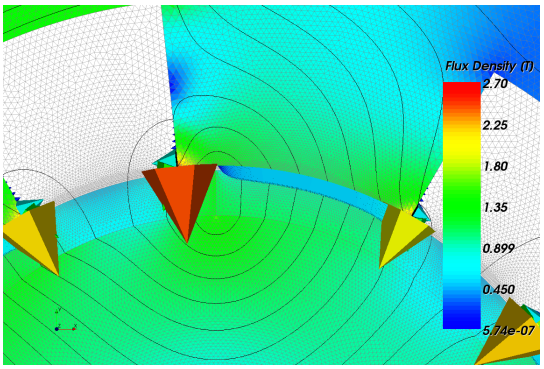

(c) Surface-force density on a fine mesh.

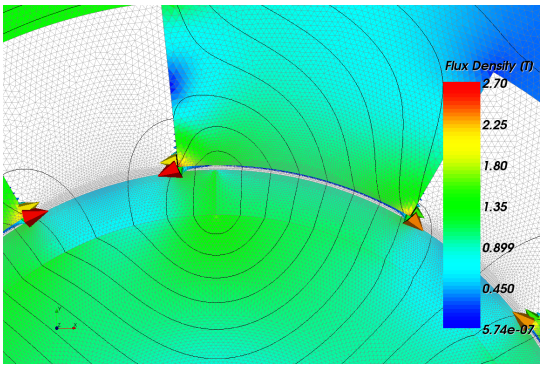

(d) Nodal forces on a fine mesh.

Fig. 2: Comparison between surface force density and nodal forces on different meshes both indicated by cones. Scale is kept constant between different meshes. The color scale and color in the background imitates the flux density amplitude.

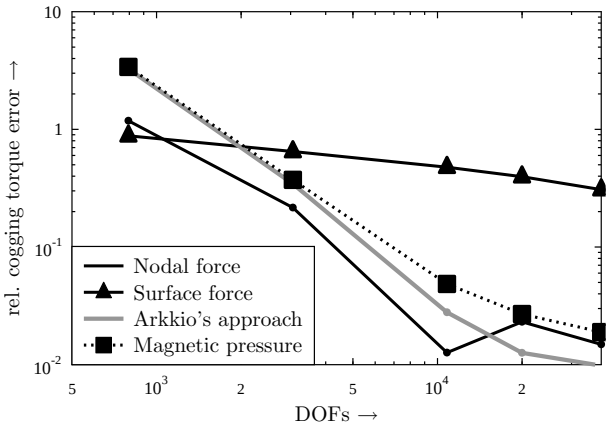

(a) No-load.

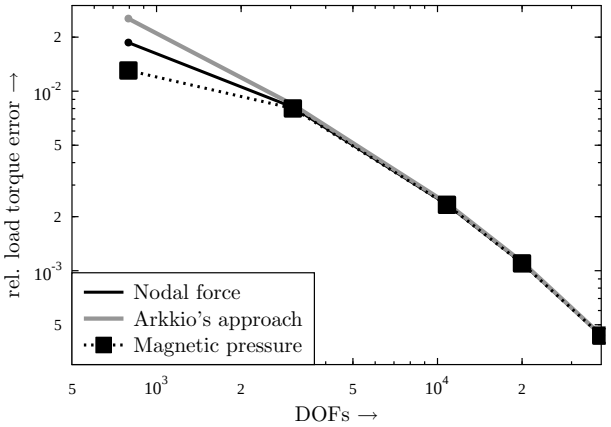

(b) Load (J =6 A/mm^2, copper fill factor 0.4).

Fig. 3: Convergence behavior of torque calculation.

where $R = \frac{D_\mathrm{i}}{2}$, $N = \frac{D_\mathrm{o}-h_\mathrm{y}}{2}$, $E = 210$ GPa, $h = h_\mathrm{y}$, $i = \frac{1}{2\sqrt{3}} \cdot \frac{h}{N}$ and all geometrical data of the machine are given in Figure 1. The advantage of this simple approach to assessing the extracted force density waves is that it can be used to calculate the mean-squared normal surface velocity of the stator by

$$\overline{|v_\mathrm{n}|^2}(\omega) = \omega^2 \sum_{r=-R}^{R} |\underline{u}_r(\omega)|^2 \ . \tag{15}$$

A question that sometimes arises, is where to sample the radial magnetic-flux density distribution to obtain radial magnetic pressure [12]. Two natural choices are: in the middle of the air gap, or exactly at the stator bore. If the latter is chosen, it is now possible to assume the field, and hence the force, to be zero between the teeth, since there is no steel, on which to act. Figure 4a visualizes this by means of the absolute value of the flux density in the air gap. It can be seen that the flux density in the middle does not have as high peaks as at the stator bore. The curve labeled "On the teeth" refers to the situation, in which the flux density is set to zero in the slot opening. Small values larger than zero in Figure 4a stem from the FOURIER decomposition. The corresponding result for forces is shown in Figure 4b. Keeping in mind that the magnetic pressure is only an approximation of the true electromagnetic force, the nodal

force approach can here be considered as a reference. For the small harmonic orders with large amplitudes the sampling location has no significant influence. Only for the higher time harmonics, which are lower in amplitude and are most like also stemming from higher space harmonics, the deviation becomes larger. In general, the evaluation in the middle of the air gap is the best option, although it might seem to be more natural to evaluate forces where they truly occur, i.e. at the stator surface. This can be explained by the fact that the magnetic pressure neglects the contribution of the electromechanical stress tensor of iron, which is larger at the saturated tooth tips. Therefore, the magnetic stress tensor, which includes the magnetic field, is lower. The physical reduction at the tooth edges is initiated by choosing the middle of the air gap, which gives less flux density although for a different reason (smoothing of the field with more distance from the singularity).

The next step is to evaluate the convergence behavior of the local force computation approaches. The mean value of surface-force density and nodal forces are taken as reference, because they are theoretically consistent and converge correctly, Figure 5a. On the other hand, the magnetic pressure gives clearly better results when evaluated in the middle of the air gap. Though an indefinite drop occurs at approx. $2 \cdot 10^5$ DOFs, the middle of the air gap variant gives significantly less error. If one wishes to develop a force calculation method aiming at analysing the acoustic radiation of the machine and how it is perceived by the human ear, it makes sense to apply an A-weighting to the results. These results are shown in Figure 5b. The picture does not change by much, except for that the total relative error becomes larger, when compared to the unweighted case. This is due to the larger uncertainties in the very small amplitudes.

To give an impression of the influence of the electromagnetic discretization on the acoustic behavior, although the structural dynamic response and acoustic radiation characteristic is not yet included, the total velocity level is calculated in dB(A). Variations with a few dB can be seen for discretizations larger than 10^4 DOFs. Considering that 1 dB is what can be considered the smallest noticeable change that can be noticed, electromagnetic force calculation with medium large discretization levels should suffice for acoustical purposes.

Another aspect, that may be important in the calculation of electromagnetic excited audible noise becomes visible, when observing the spectra of the force-density waves in time and space obtained from nodal force calculation and from surface force-density. There are harmonics that are not supposed to occur in this study case configuration, which can be derived from analytical considerations [11]. Their amplitude, so called spurious ordinal numbers, are observed to be significantly lower in the case of nodal forces, when compared to the surface-force density approach. Summing up the squared amplitude of all spurious harmonics, gives rise to the definition of the averaged squared noise terms as depicted in Figure 7. It can be seen that the nodal force approach shows the lowest averaged sqaured noise terms for reasonable discretizaiton levels. This is practically relevant, especially if comparatively small force excitations are analyzed and its is not clear if a certain force order is real or spurious. This may

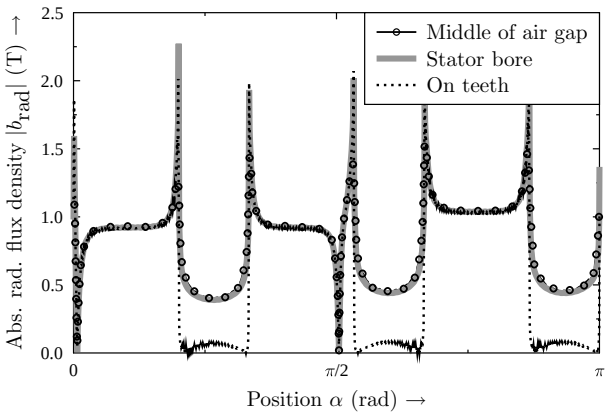

(a) Air-gap flux-density.

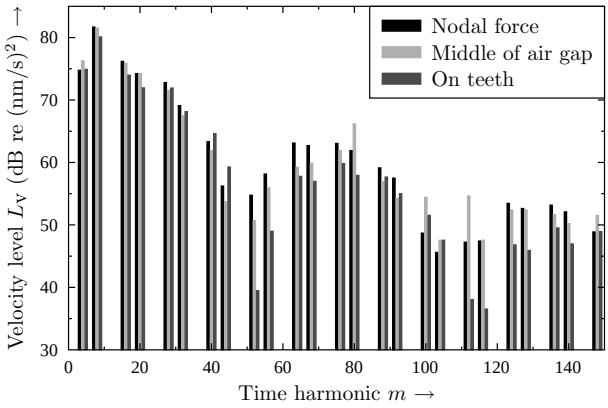

(b) Mean-squared normal surface-velocity level.

Fig. 4: Comparison of different sampling locations with the nodal force as reference.

be the case in a six-pole machine with squared outer stator surface. Naturally, in a six-pole machine only multiples of six (i.e. $r = 0, 6, 12, \ldots$) may occure in a centric model. Due to the squared outer boundary, local saturation may induce force orders of mode four and multiples thereof.

The difference in terms of numerical noise performance is also observed, even if the surface-force density is not sampled equidistantly, but a full analytical FOURIER transformation analogous to (13) is performed. It is sufficient to perform the summation of (13) only for the nodes at the interface between stator iron and air and not in the complete stator volume to obtain such a good signal-to-noise ratio. Therefore, the advantage in terms of numerical noise can solely be attributed to the nodal force approach itself, which outperforms all other methods in terms of low discretization noise.

IV. SUMMARY AND CONCLUSIONS

Four different force calculation approaches are compared in this paper: Nodal forces, surface-force density, ARKKIO'S approach and the magnetic pressure, also called MAXWELL'S stress tensor. The comparison is performed on a well defined study case geometry, based on a permanent-magnet excited synchronous machine. An evaluation parameter, the electromagnetic torque and the analytically weighted force

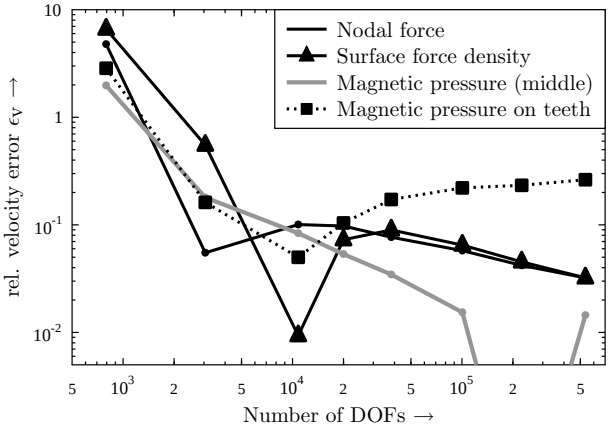

(a) Mean-squared normal surface-velocity error.

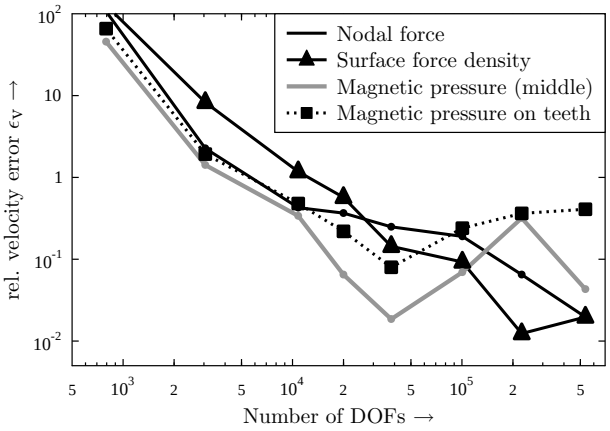

(b) A-weighted mean-squared normal surface-velocity error.

Fig. 5: Convergence behavior of local force computation.

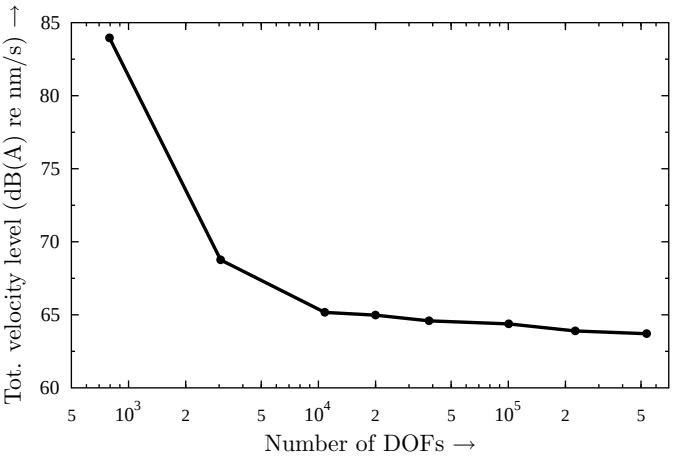

Fig. 6: A-weighted total velocity level.

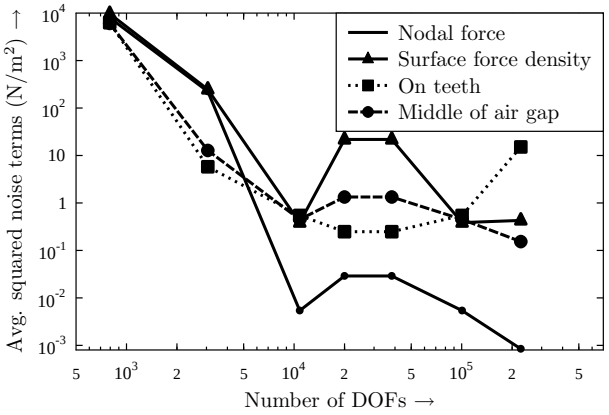

Fig. 7: Discretization noise.

amplitudes are chosen. It is found that the surface-force density is inappropriate for the calculation of torque, where it gives good results for the radial force excitation. In terms of signal-to-noise ratio, the nodal force based approach is superior. The issue of sampling location is also addressed in this paper. Sampling in the middle of the air gap is confirmed to give the best results, if the magnetic pressure is used as an approximation for the radial forces.

REFERENCES

[1] F. Henrotte, "Handbook for the computation of electromagnetic forces in a continuous medium," *International Compumag Society (I.C.S.) Newsletter, University of Southampton, U.K.*, vol. 11, no. 2, pp. 3–9, July 2004.

[2] L. Schwartz, *Théorie des distributions*. Hermann Paris, 1966.

[3] R. Kröger and R. Unbehauen, *Elektrodynamik*, 2nd ed. B.G. Teubner Stuttgart, 1990.

[4] J. Melcher, *Continuum electromechanics*. MIT Press Cambridge Massachusetts, 1981.

[5] A. Arkkio, "Time-stepping finite element analysis of induction motors," in *International Conference on Electrical Machines (ICEM)*, 1988, pp. 275–280.

[6] J. Coulomb, "A methodology for the determination of global electromechanical quantities from a finite element analysis and its application to the evaluation of magnetic forces, torques and stiffness," *IEEE Transactions on Magnetics*, vol. 19, no. 6, pp. 2514–2519, November 1983.

[7] F. Henrotte, M. Felden, M. van der Giet, and K. Hameyer, "Electromagnetic force computation with the Eggshell method," in *the 14th International Symposiumon Numerical Field Calculation in Electrical Engineering, IGTE 2010*, Graz, Austria, 2010.

[8] M. van der Giet, R. Rothe, and K. Hameyer, "Asymptotic Fourier decomposition of tooth forces in terms of convolved air gap field harmonics for noise diagnosis of electrical machines," in *the 13th International Symposiumon Numerical Field Calculation in Electrical Engineering, IGTE 2008*, Graz, Austria, 2008.

[9] J. Roivainen, "Unit-wave response-based modeling of electromechanical noise and vibration of electrical machines," Ph.D. dissertation, Helsinki University of Technology, 2009.

[10] G. Huth, "Permanent-magnet-excited AC servo motors in tooth-coil technology," *IEEE Transaction on Energy Conversion*, vol. 20, no. 2, pp. 300–307, 2005.

[11] H. Jordan, *Geräuscharme Elektromotoren*. W. Girardet, November 1950.

[12] Z. Q. Zhu, Z. Xia, L. J. Wu, and G. Jewell, "Analytical modelling and finite element computation of radial vibration force in fractional-slot permanent magnet brushless machines," in *International Electric Machines and Drives Conference, IEMDC*, Miami Florida, May 2009.